THE NORTHWARD ADVANCE OF THE SINGLE KENYA-AFAR-LEVANT PLUME HEAD

Chiara Civiero[1]*, Sergei Lebedev[1], Nicolas L. Celli[1]

(1) Dublin Institute for Advanced Studies (DIAS), Geophysics Section, 5 Merrion Square, Dublin D02 Y006, Ireland

Abstract

Buoyant plumes rising from the lower mantle have been envisaged as being warm mushroomed-shaped anomalies with a large spherical head, followed by a narrow tail. In continents, the impingement of the plumes' head at the base of the lithosphere can cause uplift, rifting and volcanism, but the head geometry and evolution remain unknown. Here, we use seismic waveform tomography to image corridors of hot mantle material flowing beneath East Africa, the Gulf of Aden, West Arabia and Middle East. The corridors underlie areas of uplift and volcanism and comprise a single, star-shaped plume head. Constraints from eruption ages and plate reconstructions suggest that it formed from south to north, and tomography shows it currently fed by three deep upwellings, the Kenya, Afar and Levant Plumes. These results demonstrate the complex feedbacks between the continental-lithosphere heterogeneity and plume-head evolution.
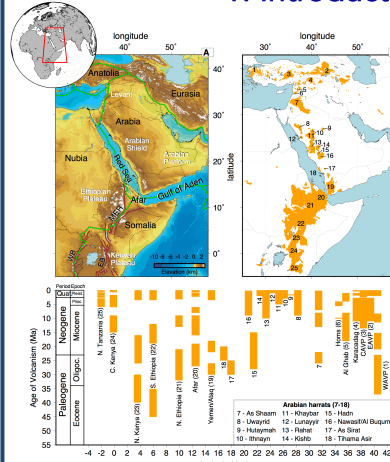
1. Introduction

Figure 1. A) Topography of the region of study. B) Location of the volcanic rocks. C) Age-latitude plot of the igneous activity.

High domes rise over 2 km in elevation.

Active volcanism throughout the process of continental breakup and rifting.

Long standing puzzle on what causes rifting, diffuse volcanism, and uplift.
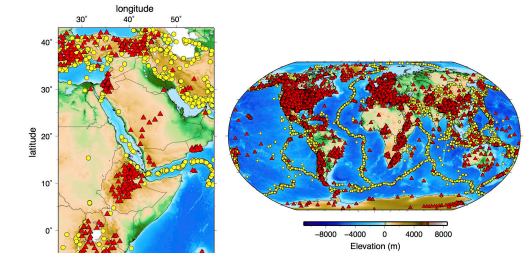
2. Dataset

Figure 2. Earthquakes and seismic stations within the study area and around the globe. Events are plotted as yellow circles, seismic broadband stations as red triangles.

The azimuthally anisotropic, S-wave speed, tomographic model is constrained by over 1.2 million seismograms, waveform-fitted using the Automated Multimode Inversion (AMI) of surface- and S-waveforms.
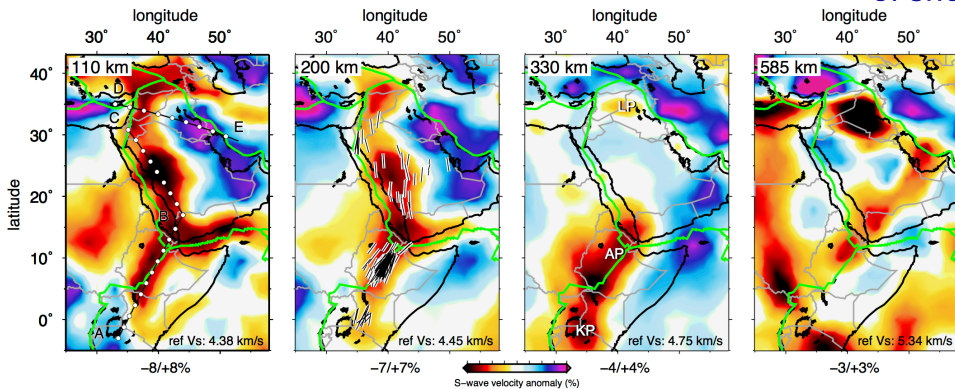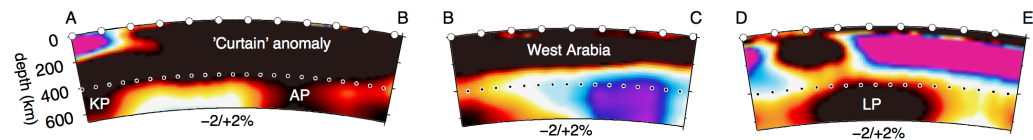
3. Shear-wave model

Figure 3. Top left panels: Depth slices of the S-wave model [*Celli et al., 2020*] at 110, 200, 330 and 585 km. The SKS splitting measurements [*Gao et al., 2010*] are plotted in the map view at 200 km depth. Right right panels: cross-sections through the main low-velocity features of the model.
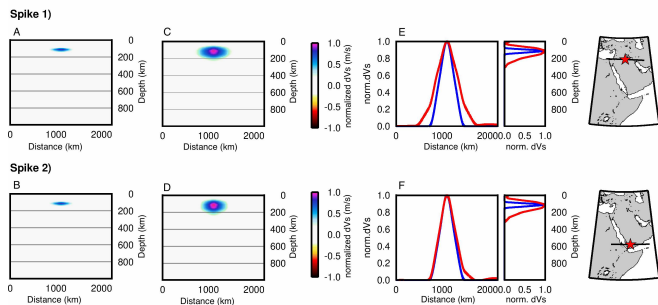
Large, star-shaped low-velocity anomaly composed of three branches:
- Curtain-like anomaly in the upper mantle below East Africa connecting Kenya and Afar Plumes.
- Low-velocity channel underlying West Arabia.
- Low-velocity anomaly following the Gulf of Aden rift.

Low-velocity anomaly extending though the transition zone below Levant region (Levant Plume).

DIAS
Institiúid Ard-Léinn | Dublin Institute for
Bhaile Átha Cliath | Advanced Studies
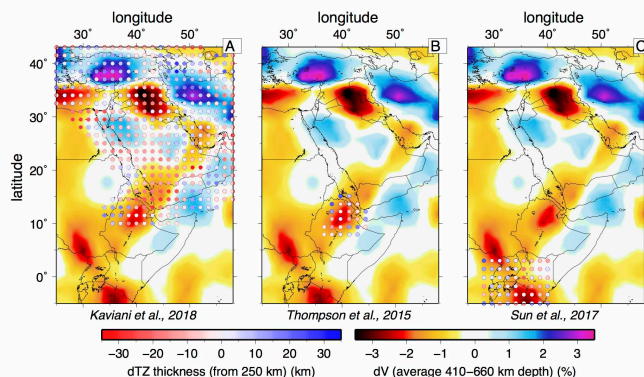
4. Resolution tests

Figure 4. Synthetic spike test. A-B) Cross-sections of the two spikes at 110 km depth through the input model. C-D) Cross-sections through the output model. Orientation of the cross-section is shown on the maps in black. E-F) Vertical and horizontal 1D *S*-wave anomaly profiles along the cross-sections.

Good recovery of synthetic structures, particularly within the upper 300 km, with our dataset.

The spurious structure as seen in the output is small and cannot be responsible for the observed anomalies.

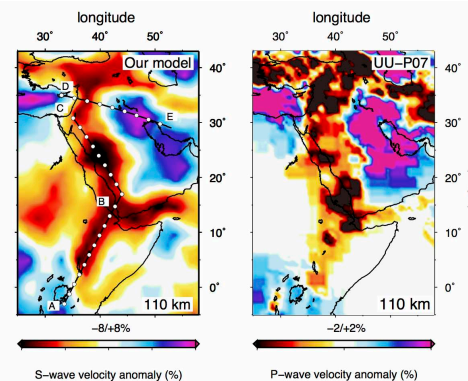Our model is capable of resolving the low-velocity features reliably.

Figure 5. 'Structural' resolution test. The low-velocity anomalies below East Africa and below the Levant region are cut off in the input at depths ≥150 km.
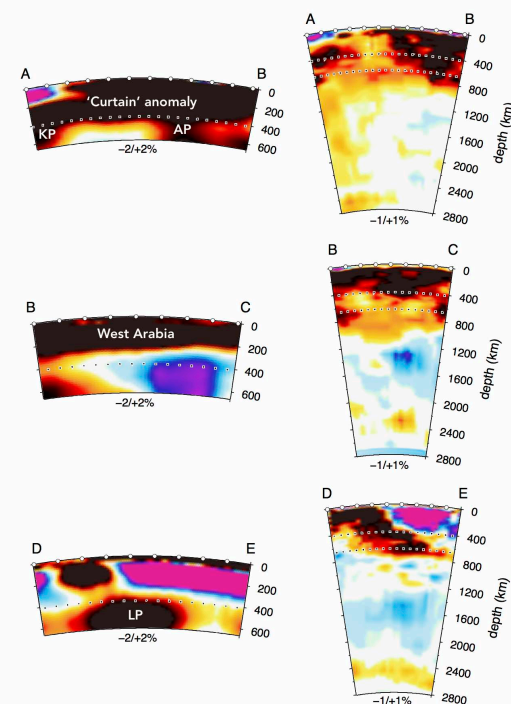
6. Transition zone thickness

Figure 7. Comparison between the average velocity anomaly and the thickness of the transition zone from published receiver functions [*Kaviani et al., 2018; Thompson et al., 2015; Sun et al., 2017*].

The elevated temperatures within the transition zone are confirmed by recent receiver function studies, which found an overall thinning of the transition zone below Ethiopia, Kenya, and Iraq.

5. Lower-mantle origin

Similar low-velocity anomalies captured by the global model UU-P07.

A broad high-velocity anomaly cuts the Levant Plume at mid-lower mantle depths (see cross sections BC and DE).

The Arabian slab, subducted during Late Cretaceous may have broken and split in different upwellings the single mantle upwelling rising from the base of the lower mantle.

Figure 6. Comparison of our tomographic model with the global P-wave model UU-P07 [*Amaru, 2007*].

7. Global models

Overall match between the low-velocity anomalies at large scales.

The higher resolution provided by our new model allows us to resolve the structure with unprecedented detail.
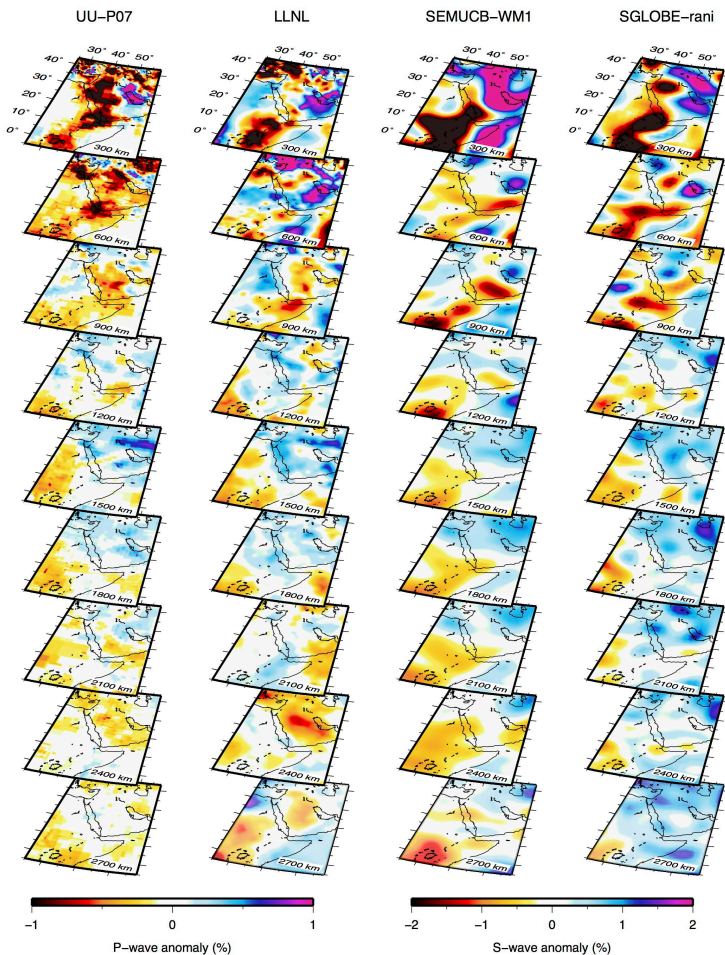
Figure 8. Global tomographic models through the whole mantle below the study region. Tomographic depth slices are shown for the following models: UU-P07 [*Amaru, 2007*]; LLNL [*Simmons et al., 2012*]; SEMUCB-WM1 [*French and Romanowicz, 2014*]; SGLOBE-rani [*Chang et al., 2015*].
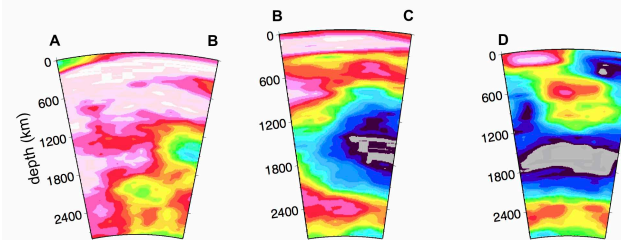
8. Vote maps and cross sections
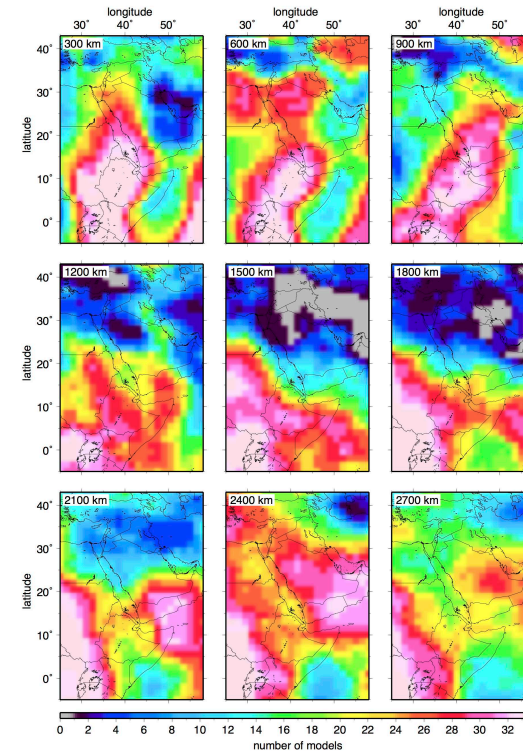
Figure 9. Low-velocity vote maps for 34 tomographic models (dv/v < 0). The voting maps are obtained stacking *P*- and *S*-wave models available in the *SubMachine* tomography web portal [*Hosseini et al. 2018*].

Figure 10. Low-velocity cross-sections for 34 tomographic models (dv/v < 0). The cross-sections are the same as those of our model.

Maximum-vote region below East Africa, capturing well the shape and extent of the 'curtain-like' anomaly.

The low-velocity channel below Western Arabia is identified with a high-vote elongated area, which appears as a continuation of the low-velocity curtain below East Africa.

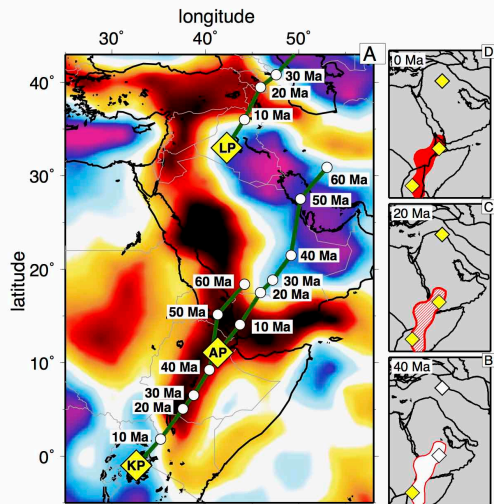High level of consistency in assigning low velocities predominantly in two main clusters:
• under offshore Somalia and Arabia;
• beneath East and Central Africa.

High votes are observed below Iraq in agreement with our tomographic images, which show a strong low-velocity anomaly, interpreted as the tail of the Levant mantle plume.

DIAS Institiúid Ard-Léinn | Dublin Institute for
Bhaile Átha Cliath | Advanced Studies

9. Plate reconstruction

Figure 11. Predicted hotspot tracks. A) Tracks of the Afar plume (AP), Kenya plume (KP) and Levant plume (LP) relative to Arabian plate according to the reference frame of *Torsvik et al. [2019]*. The track is extended back to 60 Ma. White dots along tracks are in 10 Myr intervals. The three plumes are indicated with yellow diamonds.

The Kenya Plume was below Ethiopia at 40-50 Ma.

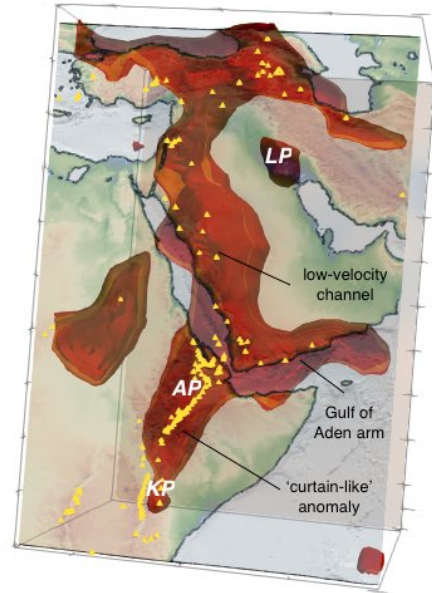No old volcanism below Arabia associated with the Afar Plume.

The Kenya Plume may have initiated volcanism in Ethiopia while the Afar plume was still rising in the lower mantle below Arabia.

The curtain formed between the Kenya Plume in the south and the Afar Plume in the north.

Acknowledgements

10. Summary

Figure 12. Three-dimensional view of three-pronged East Africa-Middle East plume head. Low-velocity at -2% are plotted in the upper mantle.

✓ Intraplate volcanism in East Africa-Middle East fed by at least three deep upwellings, the Kenya, Afar and Levant Plumes forming a single living head.

✓ Star-shaped non–convex plume heads may be more common than we thought.

✓ Complex feedback between the channeling of hot material in thinner-lithosphere areas, and the thinning of the lithosphere due to the arrival of the plume.

✓ This mechanism of plume-continent dynamics can be occurring in many areas affected by continental rifting (e.g., North Atlantic, CAMP magmatism).

References

1. N. L. Celli, L. Lebedev, A. J. Schaeffer, C. Gaina, *Nat. Commun.* **11**, 92 (2020).
2. S. S. Gao, K. H. Liu, M. G. Abdelsalam, *J. Geophys. Res. Solid Earth.* **115**, 1–15 (2010).
3. A. Kaviani, E. Sandvol, A. Moradi, G. Rümpker, Z. Tang, P. M. Mai, *J. Geophys. Res. Solid Earth.* **123**, 4886–4905 (2018).
4. D. A. Thompson, J. O. S. Hammond, J-M. Kendall, G. W. Stuart, G. Helffrich, D. Keir, A. Ayele, B. Goitom, *Geochem. Geophys. Geosyst.* **16**, 834–846 (2015).
5. M. Sun, K. H. Liu, X. Fu, S. S. Gao, *Geophys. Res. Lett.* **44**, 12116–12124 (2017).
6. M. L. Amaru, *Geol. Ultraiectina.* 274, 174 (2007).
7. N. A. Simmons, S. C. Myers, G. Johannesson, E. Matzel, *J. Geophys. Res. Solid Earth.* **117**, B10302 (2012).
8. S. W. French, B. A. Romanowicz, *Geophys. J. Int.* **199**, 1303–1327 (2014).
9. S. Chang, A. M. G. Ferreira, J. Ritsema, H. J. Heijst, J. H. Woodhouse, *J. Geophys. Res. Solid Earth.* **120**, 4278–4300 (2015).
10. K. Hosseini, K. J. Matthews, K. Sigloch, G. E. Shephard, M. Domeier, M. Tsekhmistrenko, 2018. Geochem. Geophys. Geosyst. **19**, 1464–1483 (2018).
11. T. H. Torsvik, B. Steinberger, G. E. Shephard, P. V. Doubrovine, C. Gaina, M. Domeier, C. P. Conrad, W. W. Sager, Geochem. Geophys. Geosyst. **20**, 3659–3689 (2019).

DIAS
Institiúid Ard-Léinn | Dublin Institute for
Bhaile Átha Cliath | Advanced Studies